JMEPEG (1992) 1:813-822

Superplastic Sheet Metal Forming of a Generalized Cup Part II: Nonuniform Thinning

N. Chandra and D. Kannan

A computational process model for the superplastic formation of a generalized cup is presented that takes into account the variation in thinning in the unsupported region. The relative pole to edge thinning arises due to the change in the state of stress from balanced biaxial at the pole to plane strain at the edge. Using kinematic conditions and material constitutive equations, a relationship between the instantaneous thickness at the pole and edge is developed. An equation for thickness variation from center to edge in terms of convected coordinates is postulated. Process parameters including thickness profile and pressure-time cycle for the generalized cup are determined using an incremental formulation. The solution developed in Part II depends on process and material parameters, unlike the uniform thinning model. The thickness profile for different shapes like the dome, cup, and cone formed from superplastic aluminum 7475 and aluminum-lithium alloys are compared with experimental results.

1. Introduction

SUPERPLASTIC forming (SPF) has been established as one of the advanced techniques of fabricating complex components in the aerospace and automotive industries. In Part I of this article, a closed form solution to describe the superplastic forming of a generalized cup was developed.[1] The mechanics of deformation was based on the assumption that the thickness of the sheet in the free region is uniform. However, as will be shown in Part II, this assumption is not exact, as observed in experiments.[2-11] The nonuniform thickness distribution introduces substantial changes in the formulation of the model.

Jovane[2] was one of the first researchers to assume uniform thinning on a dome, but reported that there was a variation in thickness in a tin-lead alloy when formed superplastically at room temperature. He observed experimentally that the thickness variation increased with deformation (higher total strain) and decreased with an increase in m value (more superplastic). Holt[3] considered the variation in thickness by measuring the slope of the dome at the circumferential edge and assuming a balanced biaxial state throughout the domain. Cornfield and Johnson[4] formulated a numerical iterative technique to account for the thickness variation. They assumed that a state of balanced biaxial stress exists throughout the sheet, but readjusts at the edge. Their numerical model indicated that the deviation from uniform thickness model increased with a decrease in m value. Al-Hassani[5] assumed that material points travel along circular arcs with edge as the center and arrived at the thickness variation. This assumption produces a balanced biaxial everywhere. He considered the variation of material parameters K and m as a function of local strain. It will be shown later that, if a balanced biaxial state is assumed everywhere, it leads to no change in thickness at the edge, which is contrary to experimental observations.

N. Chandra and **D. Kannan**, Mechanical Engineering Department, Florida A&M University, Florida State University, Tallahassee, Florida.

Guo *et al.*[6] analyzed bulge forming of superplastic aluminum 7475 alloy using a stress ratio based on plastic hole growth. Ghosh and Hamilton[7] conducted bulge tests on Ti-6Al-4V and aluminum 7475 alloy. In their analytical model,

Notations

a	Radius of the die opening
h	Height of the pole from initial position
H	Total height of the cup
m	Strain-rate sensitivity factor
k	Material constant
P	Pressure of forming
s	Current thickness
s_0	Initial thickness
s_p	Thickness at the pole
s_e	Thickness at the edge
$s_e$new	Edge thickness at time $t + \delta t$
$s_e$old	Edge thickness at time δt
t	Time
V	Volume at any instant
V_0	Initial volume
dV	Infinitesimal change in volume
1,2,3 (subscript)	Meridian, circumferential, and thickness direction
α	Ratio of σ_2 to σ_1
β	Ratio of ε_2 to ε_1
$\bar{\dot{\varepsilon}}$	Effective strain rate
$\dot{\varepsilon}_{3p}$	Thickness strain rate at the pole
$\dot{\varepsilon}_{3e}$	Thickness strain rate at the edge
$\bar{\sigma}_p$	Effective stress at the pole
$\bar{\sigma}_e$	Effective stress at the edge
σ_1	Stress along the meridian direction
σ_2	Stress along the circumferential direction
σ_{1p}	Meridional stress at the pole
σ_{1e}	Meridional stress at the edge
ρ	Radius of curvature of the spherical segment
θ	Angle formed at the center of curvature starting from the pole
δt	Time step
φ	Total angle of formation at the center of curvature

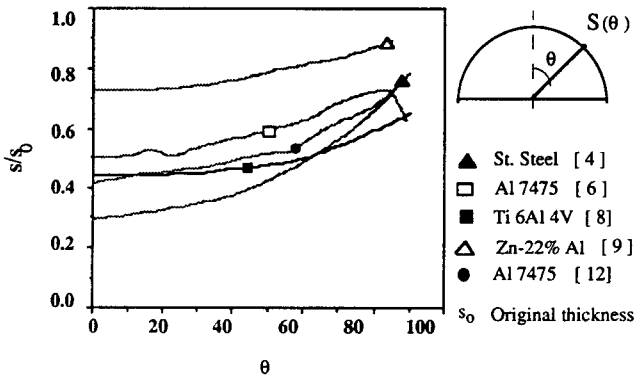

Fig. 1 Variation in thickness with angle in a hemispherical dome.

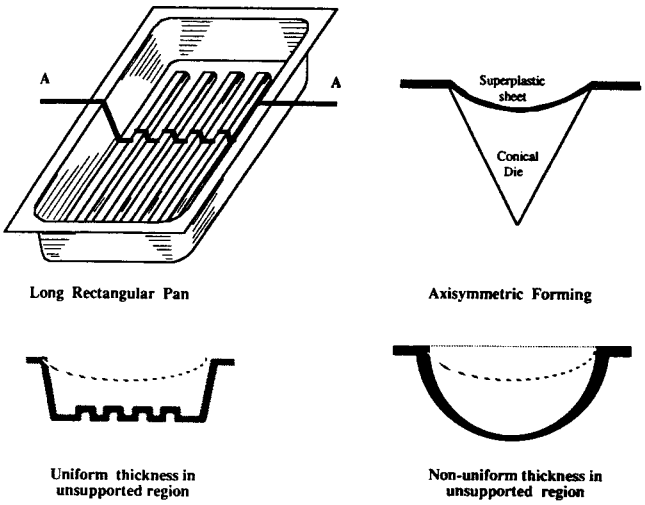

Fig. 2 Thickness distribution in long rectangular box and axisymmetric component.

they assumed a parabolic thinning ratio based on experimental observation. Other works have been variations of the above models.[8-11] Experimental results of the variation in thickness of a hemispherical dome for different materials are shown in Fig. 1. In all of the theoretical models, a spherical shape of deformation is assumed.[2-11] This assumption is validated through experimental works.[5,6,12]

It is evident from the above discussion that there is a thickness variation due to a change in stress state from balanced biaxial at the pole (geometric center of the free region) to plane-strain at the edge (where the sheet is in circumferential contact with the die). In Part II of this article, this thickness variation is accounted for in the formulation and solution to the generalized cup problem. In this analysis, the power-law model

$$\sigma = K \dot{\varepsilon}^{m} \qquad [1]$$

is used with a unique value of m and K. However, the values of m and K may vary with $\dot{\varepsilon}$, leading to a different flow stress. In this article, the variation of state of stress at a different radial

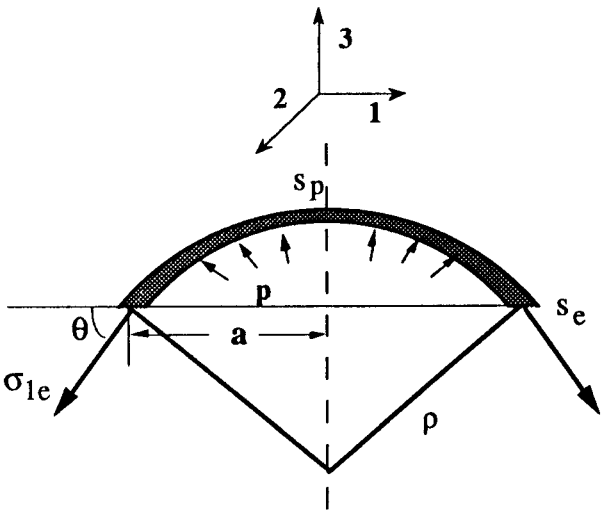

Fig. 3 Free bulge forming.

distance from the pole at any given stage of formation is considered in arriving at the thickness distribution.

2. Analysis of a Free-Forming Dome

In the formation of a rectangular pan, if the length is considerably larger than the width, then a state of plane-strain exists in the middle section of the box,[13] because the strain along the major axis is negligible, as shown in Fig. 2. When such a plane-strain condition exists, uniform thickness reduction occurs, which has been shown experimentally and theoretically.[13] However, in any axisymmetric part, the center is in a state of balanced biaxial strain, and the clamped edge is in a state of plane-strain. This variation of strain state causes differential thinning in a free-forming part, as shown in Fig. 2. In this figure, dotted lines show the unsupported region in both cases. At any instant, the unsupported region in the plane-strain box will be of uniform thickness, whereas the axisymmetric component will have nonuniform thickness. Any analysis other than the simple long rectangular box should incorporate the nonuniform thinning. The relative pole to edge thinning depends on the instantaneous value of the pole and edge thicknesses, strain-rate sensitivity, and the pressure loading. Because at various stages of the formation of an axisymmetric component the free-forming region (except the last) assumes the shape of a spherical segment, the analysis of a dome is critical in the process model of a generalized cup.

Consider a circular sheet clamped at the edge and subjected to a gas pressure P as shown in Fig. 3. The hoop stress at the pole is given by:

$$\sigma_{1p} = \frac{P\rho}{2s_p} \qquad [2]$$

where σ is the stress, ρ is the radius of curvature, and s is the thickness. The subscripts 1, 2, and 3 refer to meridional, cir-

cumferential, and the thickness directions, respectively, and are used for stress and strain quantities; the other subscripts p and e correspond to the values at the pole and the edge.

Balancing the force in the vertical direction (Fig. 3):

$$2\pi a s_e \sigma_{1e} \sin\theta = \pi a^2 P \qquad [3]$$

$$\sigma_{1e} s_e = \frac{P\rho}{2} \qquad [4]$$

where

$$a = \rho \sin\theta \qquad [5]$$

From Eq 2 and 4:

$$\sigma_{1p} s_p = \sigma_{1e} s_e \qquad [6]$$

From the condition of plane-strain at the edge:

$$\sigma_1 = 2\sigma_2 \qquad \alpha \equiv \frac{\sigma_2}{\sigma_1} = \frac{1}{2} \qquad [7a]$$

$$\dot{\varepsilon}_2 = 0 \qquad \beta \equiv \frac{\dot{\varepsilon}_2}{\dot{\varepsilon}_1} = 0 \qquad [7b]$$

Using von Mises criteria:

$$\sigma_{1e} = \frac{2}{\sqrt{3}} \bar{\sigma}_e \qquad \dot{\bar{\varepsilon}}_e = \frac{2}{\sqrt{3}} \dot{\varepsilon}_{1e} = -\frac{2}{\sqrt{3}} \dot{\varepsilon}_{3e} \qquad [8]$$

Similarly at the pole with a balanced biaxial condition:

$$\sigma_1 = \sigma_2 \qquad \alpha = \frac{\sigma_2}{\sigma_1} = 1 \qquad [9a]$$

$$\dot{\varepsilon}_2 = \dot{\varepsilon}_1 \qquad \beta = \frac{\dot{\varepsilon}_2}{\dot{\varepsilon}_1} = 1 \qquad [9b]$$

$$\sigma_{1p} = \bar{\sigma}_p \qquad \dot{\bar{\varepsilon}}_p = 2\dot{\varepsilon}_{1p} = -\dot{\varepsilon}_{3p} \qquad [10]$$

Using constitutive equations at the pole and the edge:

$$\bar{\sigma}_p = k \dot{\bar{\varepsilon}}_p^m \qquad \bar{\sigma}_p = k(-\dot{\varepsilon}_{3p})^m \qquad [11]$$

$$\bar{\sigma}_e = k \dot{\bar{\varepsilon}}_e^m \qquad \bar{\sigma}_e = k\left(-\frac{2}{\sqrt{3}}\dot{\varepsilon}_{3e}\right)^m \qquad [12]$$

From Eq 6, the ratio of thickness at the pole and the edge can be written as:

$$\frac{s_p}{s_e} = \frac{\sigma_{1e}}{\sigma_{1p}} \qquad [13]$$

The above equation can also be expressed in terms of thickness strain rates as:

$$\frac{s_p}{s_e} = \frac{2}{\sqrt{3}} \left(\frac{\frac{2}{\sqrt{3}} \dot{\varepsilon}_{3e}}{\dot{\varepsilon}_{3p}} \right)^m \qquad [14]$$

If ${}^{t+\delta t} s_e$ is the deformed thickness at $t + \delta t$ and ${}^{t} s_e$ is the thickness at the edge at time t with an incremental time period δt, then the incremental thickness strain $\delta \varepsilon_{3e}$ at the edge is

$$\delta \varepsilon_{3e} = \left[\ln \left(\frac{t + \delta t_{s_e}}{t_{s_e}} \right) \right] \qquad [15]$$

and the incremental strain rate is

$$\delta \dot{\varepsilon}_{3e} = \frac{d(\delta \varepsilon_3)}{dt} = \frac{1}{\delta t} \ln \left[\frac{t + \delta t_{s_e}}{t_{s_e}} \right] \qquad [16]$$

Substituting in Eq 14:

$$\frac{t + \delta t_{s_p}}{t + \delta t_{s_e}} \equiv \frac{s_p}{s_e} = \left(\frac{2}{\sqrt{3}} \right)^{(1+m)} \left(\frac{1}{\dot{\varepsilon}_{3p} \delta t} \right)^m \left[\ln \left(\frac{t + \delta t_{s_e}}{t_{s_e}} \right) \right]^m \qquad [17]$$

If the optimum value of $\dot{\bar{\varepsilon}}$ is maintained at the pole, then $\dot{\varepsilon}_{3p}$ is fixed. Then from the above equation, the thickness ratio s_p/s_e can be obtained as a function of deformation, as shown in Fig. 4. As shown in the figure, the ratio decreases with deformation, indicating that the pole is thinning faster than the edge. This ratio of s_p/s_e is affected more by a decrease in m (less superplastic materials), and thus, materials with lower m values will have more nonuniform thinning. Also for any given material (m = constant), the ratio s_p/s_e decreases with deformation. Numerical expressions show that the s_p/s_e ratio is not affected by imposed strain rate at the pole $\dot{\bar{\varepsilon}}_p$ or by the actual value of initial thickness. It should be noted that Eq 17 specifies only the ratio of the thickness at the pole and the edge and does not provide any information on the distribution of thickness between them.

To complete the description of the deformation, the thickness at various regions needs to be known for the calculation of volume and the imposition of the incompressibility condition. Only then can the depth at the pole and other kinematic quantities can be calculated. In this work, it is postulated that the thickness at any point in the domain depends on its convected distance along the plane of the sheet from the geometric center. In the case of a dome, the thickness depends on the arc length from the pole, *i.e.*, $s \propto$ arc length, or $s \propto \theta$ with the condition that at $\theta = 0$, $s = s_p$ and $s = s_e$ at $\theta = \varphi$, as shown in Fig. 5. Thus:

$$s = \left[s_p - \left(\frac{\theta}{\varphi} \right) (s_p - s_e) \right] \qquad [18]$$

The above equation can be interpreted as assuming a linear variation in thickness from pole to edge with the linearity as a

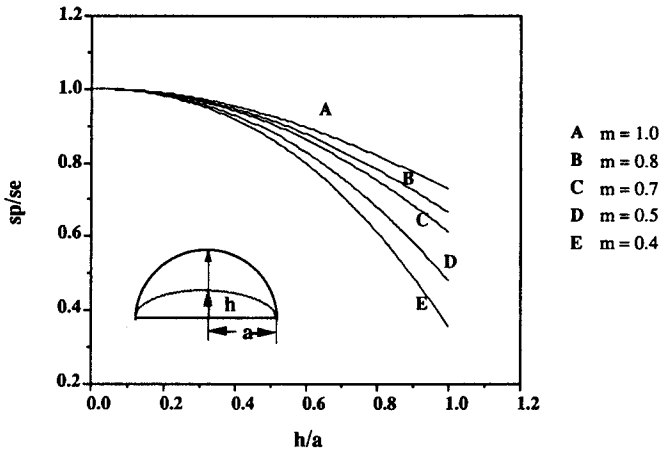

Fig. 4 Comparison of $\frac{s_p}{s_e}$ with $\frac{h}{a}$ for various m values.

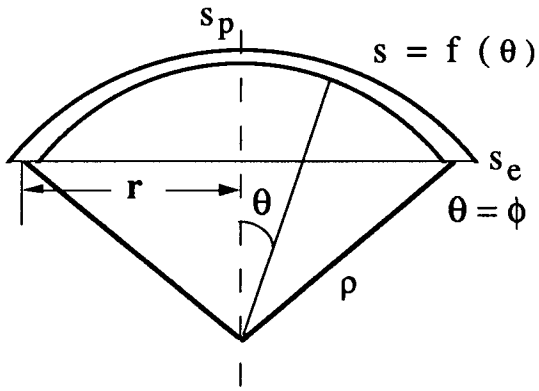

Fig. 5 Dome forming.

function of convected (deformed) length along the sheet. The above equation is also motivated from the experimental observation that there is a linear correlation between s and angle θ for a variety of materials, as shown in Fig 1. Incorporating Eq 18 into Eq 17, it is possible to calculate the strain rate ratio $\beta = \frac{\dot{\varepsilon}_2}{\dot{\varepsilon}_1}$ and stress ratio $\alpha = \frac{\sigma_2}{\sigma_1}$ at any point in the domain. It should be noted that from the specified boundary conditions at the pole $\alpha = \beta = 1$ and at the edge $\alpha = \frac{1}{2}$ and $\beta = 0$, and the variation between the pole and the edge causes the nonuniformity in thinning. Figure 6 shows the consequence of thickness variation Eq 18 on the stress ration α and strain ratio β when the dome is hemispherical. It can be seen that the state of balanced biaxial ($\alpha = 1$) prevails around the pole and changes to plane-strain ($\alpha = 0.5$) gradually. Similar variation is also observed for strain ratio β. However, if one assumes a state of balanced biaxial stress everywhere ($\alpha = 1$), then at the edge also ($\beta = 1$); in such a case, $\varepsilon_1 = \varepsilon_2 = 0$ because the circumferential strain $\varepsilon_2 = 0$. From the incompressibility condition $\varepsilon_3 = -(\varepsilon_1 + \varepsilon_2) = 0$, there will be no thinning at all at the edge, which is incorrect.

Equation 14 can be rewritten as:

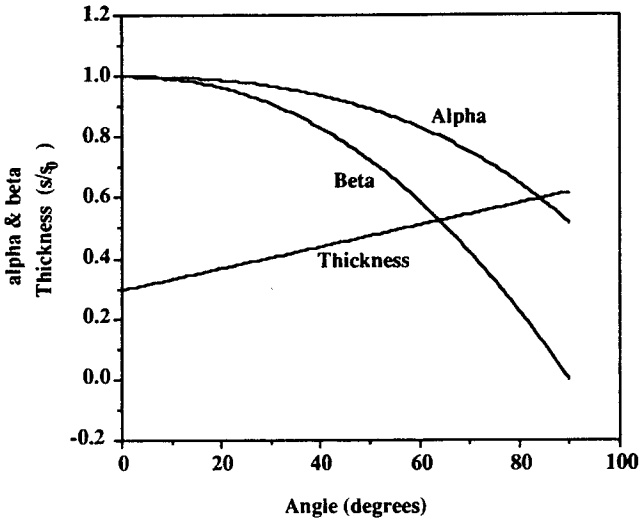

Fig. 6 α and β variation from pole to edge in free bulge forming.

$$\frac{s_p}{s_e} = \left(\frac{2}{\sqrt{3}}\right)^{(1+m)} \left(\frac{\dot{\varepsilon}_{3e}}{\dot{\varepsilon}_{3p}}\right)^m \quad [19]$$

Interestingly, even the uniform thickness distribution (s = constant) yields different strain rates $\dot{\varepsilon}$ at the edge and the pole.[1,2] When $s_p = s_e$, the above equation shows that the thickness strain rate at the edge and the pole are different, indicating that uniform thickness cannot exist any further. Thus, the above discussion gives theoretical evidence of thickness variation, purely based on the variation of state of strain from pole to edge.

For a given radius (a) and initial thickness (s_0), the initial volume is

$$V_0 = \pi a^2 s_0 \quad [20]$$

and the instantaneous volume of the spherical segment of angle φ is given as:

$$dV = 2\pi a \rho \, d\theta \, s = 2\pi \rho \sin\theta \, \rho \, d\theta \, s \quad [21]$$

Integrating the differential volume over the curvature limit 0 to φ

$$V = 2\rho\rho^2 \int_0^{\varphi} \sin\theta \, s \, d\theta \quad [22]$$

Using the thickness variation in Eq 18:

$$V = 2\pi\rho^2 \int_0^{\varphi} \sin\theta \left[s_p - \left(\frac{\theta}{\varphi}\right)(s_p - s_e) \right] d\theta \quad [23]$$

$$V = 2\pi\rho^2 \left[\int_0^{\varphi} \sin\theta \, s_p \, d\theta - \int_0^{\varphi} \left(\frac{\theta}{\varphi}\right)(s_p - s_e)\sin\theta \, d\theta \right] \quad [24]$$

Integrating and equating with the original volume equation (Eq 20):

$$s_0 = 2\left(\frac{1}{\sin\varphi}\right)^2\left[s_p(1-\cos\varphi) - \left(\frac{s_p - s_e}{\varphi}\right)[-\varphi\cos t\,\varphi + \sin\varphi]\right] \quad [25]$$

Thickness at the pole is obtained from:

$$s_p = s_0 \cdot e^{-(\varepsilon_{3p})} \qquad \varepsilon_{3p} = \dot{\varepsilon}_{3p} \cdot (t + \delta t) \quad [26]$$

Knowing s_p, s_e can be calculated from Eq 17. Because s_0, s_p, and s_e are known, angle φ can be evaluated from Eq 25. Using angle φ, various geometric quantities can be determined.

3. Generalized Cup

The different stages of formation of a generalized cup are described in Fig. 7. The nonuniform thinning model developed in the earlier section is used to analyze all of the stages of generalized cup formation. An incremental formulation is used in the numerical scheme to calculate the kinematic and kinetic quantities. It is assumed that all the quantities are known at time t, and the quantities at time $t + \delta t$, after an incremental time δt, need to be evaluated. Once quantities are known at $t + \delta t$, the procedure can be repeated for the next time increment and so on. A left superscript indicates the time of evaluation, thus $^t()$ indicates the quantity ( ) referred to at time t.

3.1 *Stage I*

During stage I ($0 \le h \le h_1$), the sheet deforms into a spherical segment until it contacts the side wall. For a draft angle of α, the spherical segment will deform until it subtends an angle $\frac{\pi}{2} - \alpha$ at the center of the curvature. In stage I, given a strain rate ($\dot{\varepsilon}$), strain-rate sensitivity (m), and initial thickness (s_0), thickness at the pole (s_p) is obtained from:

$$s_p = s_0 \cdot e^{-(\varepsilon_{3p})} \qquad \varepsilon_{3p} = \dot{\varepsilon}_{3p} \cdot (t + \delta t) \quad [27]$$

The analysis is performed in time steps of δt starting from a flat circular superplastic sheet. Once thickness at the pole (s_p) is known, using the following equation:

$$\frac{s_p}{s_e} = \left(\frac{2}{\sqrt{3}}\right)^{(1+m)}\left(\frac{1}{\dot{\varepsilon}_{3p}\delta t}\right)^m\left[\ln\left(\frac{t + \delta t_{s_e}}{t_{s_e}}\right)\right]^m \quad [28]$$

thickness at the edge can be evaluated. Thickness at the edge and pole at any instant of time can be related to the geometry of deformation using Eq 25. The angle φ included by the spherical segment at the center can be obtained by solving equation:

$$s_0 = 2\left(\frac{1}{\sin\varphi}\right)^2\left[s_p(1-\cos\varphi) - \left(\frac{s_p - s_e}{\varphi}\right)[-\varphi\cos\varphi = \sin\varphi]\right] \quad [29]$$

using Newton's method. From the angle φ and die radius a, the radius of curvature ρ and height of spherical segment q are obtained using:

$$\rho = \frac{a}{\sin\varphi} \quad [30]$$

$$q = \rho - \sqrt{\rho^2 - a^2} \quad [31]$$

The maximum height of deformation during stage I is

$$h_1 = a\frac{(1-\sin\alpha)}{\cos\alpha}$$

At the end of every time step in stage I, the pole height is checked to determine whether the material has contacted the side walls, *i.e.*, if the total height of deformation $h_1 \le q$. Thickness strain rate at the edge is obtained from the relation:

$$\dot{\varepsilon}_{3e} = \frac{1}{\delta t}\left[\ln\left(\frac{t + \delta t_{s_e}}{t_{s_e}}\right)\right] \quad [32]$$

and pressure from

$$P = \frac{2\sigma_{1p}s_p}{\rho} = \frac{2\sigma_{1e}s_e}{\rho} \quad [33]$$

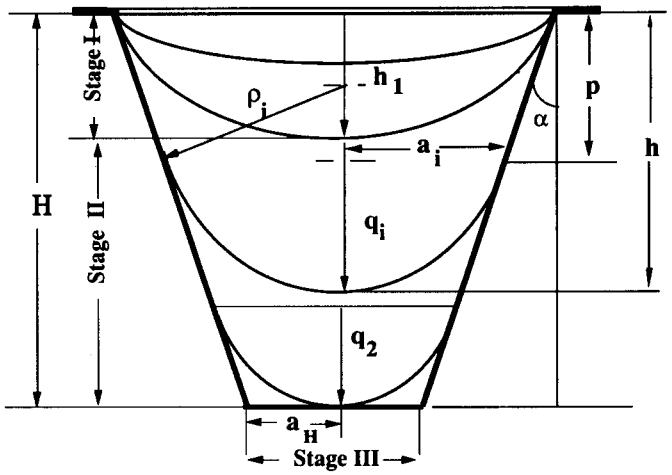

Fig. 7 Stage of deformation of a generalized cup.

It is assumed that the radius of curvature is the same throughout the spherical segment.

3.2 *Stage II*

During stage II ($h_1 \le h \le H$), the unsupported sheet metal or spherical segment is assumed to deform as part of a spherical segment. Hence, for every time increment, s_p is calculated and then s_e is found using the same set of equations for stage I. During stage II, the unsupported region further deforms as part of a spherical segment; hence, the new thickness at the pole and the edge can be obtained using the equations for s_p and $\frac{s_p}{s_e}$. The thickness at the point of contact of the sheet with the side wall after a time δt and the height of formation along the side wall δp during the same time δt is evaluated by means of Newton's method from a set of equations given below. There are seven unknowns ${}^{t+\delta t}a$, dh, ${}^{t+\delta t}\rho$, q, s'_e, ${}^{t+\delta t}V_{\text{cone}}$ and ${}^{t+\delta t}V_{\text{dome}}$ and seven different equations to solve, to provide the geometric quantities:

$$ {}^{t+\delta t}a = ({}^{t}a - \delta p \cdot \tan\alpha) \qquad [34] $$

$$ {}^{t+\delta t}\rho = \frac{{}^{t+\delta t}a}{\cos\alpha} \qquad [35] $$

$$ {}^{t+\delta t}q = {}^{t+\delta t}\rho - \sqrt{[({}^{t+\delta t}\rho)^2 - ({}^{t+\delta t}a)^2]} \qquad [36] $$

$$ s'_e = s_e - \frac{(s_e - s_p)\cdot\delta p}{\delta p + q} \qquad [37] $$

$$ {}^{t+\delta t}V_{\text{cone}} = \pi \cdot ({}^{t+\delta t}a + {}^{t}a) \cdot \frac{\delta p}{\cos\alpha} \cdot \frac{s_e + s'_e}{2} \qquad [38] $$

$$ {}^{t+\delta t}V_{\text{dome}} = {}^{t}V_{\text{dome}} - {}^{t+\delta t}V_{\text{con}} \qquad [39] $$

$$ {}^{t+\delta t}V_{\text{dome}} = 2\pi\rho^2\left[s_p(1-\cos\gamma) - \left(\frac{s_p - s_e}{\gamma}\right)[-\gamma\cos\gamma + \sin\gamma]\right] \qquad [40] $$

where $\gamma = \frac{\pi}{2} - \alpha$, s_e is the edge thickness of spherical segment at time t, ${}^{t+\delta t}\rho$ is the new radius of curvature, ${}^{t+\delta t}a$ is the new radius of the spherical segment, and s'_e is the edge thickness of spherical segment at time $t + \delta t$ in stage II. The above set of equations is solved using iterative methods for obtaining the verticle height δp of the truncated cone formed in stage II during the time step δt. The thickness distribution is calculated until the sheet contacts the bottom wall. These equations were solved using the symbolic language *Mathematica*. Given the material properties and geometric configuration, the program evaluates the thickness distribution and pressure-time cycle.

3.3 *Stage III*

During stage III ($0 \le r \le a_H$), the unsupported region deforms as part of a toroidal segment, and the volume of a toroidal segment formed during stage III is expressed in terms of r, which is derived in Section 3 of Part I. The bottom radius of the cup is a_H, which is given by $a - H\tan\alpha$. The variable r is the distance about which the deformation has taken place along the bottom wall, and r_s is the radius of curvature along the meridion direction of the toroidal segment. The same method of formulation, except for the variation in thickness, will be used here. The volume of a toroidal segment with s_p and s_e as the thicknesses at the two points of contact on the surface is given by:

$$ V_r = 2\pi r r_s\left[s_e\frac{\pi}{2} - s_p\alpha - (s_e - s_p)\frac{\left(\frac{\pi}{2}+\alpha\right)}{2}\right] + 2\pi r_s^2\left[s_p - s_e\sin\alpha + \frac{s_e - s_p}{\left(\frac{\pi}{2}-\alpha\right)}\cos\alpha\right] \qquad [41] $$

The volume of the material laid on the side wall is given as:

$$ V_s = \pi(2a_2 - r\sin\alpha)r\,\frac{\left(t + \delta t_{s_e} + t_{s_e}\right)}{2} \qquad [42] $$

where a_2 is the radius of the cup at the end of stage II. The volume of the material laid over the bottom surface is given as:

$$ V_b = \pi r^2\,\frac{\left(t + \delta t_{s_p} + t_{s_p}\right)}{2} \qquad [43] $$

The new edge and pole thicknesses ${}^{t+\delta t}s_e$ and ${}^{t+\delta t}s_p$ are obtained using Eq. 26. It is assumed that during stage III the material thinning is uniform all over the surface. Consequently, Eq 26 is applied to the edge thickness s_e also. The initial volume V_2 of the material at the start of stage III is obtained from Eq 25 as:

$$ V_2 = 2\pi\rho_2^2\left[s_p(1-\cos\varphi) - \left(\frac{s_p - s_e}{\varphi}\right)[-\varphi\cos\varphi + \sin\varphi]\right] \qquad [44] $$

where $\varphi = \frac{\pi}{2} - \alpha$. Once the new thicknesses are found, the height or radius of deformation is obtained using the volume equivalents:

$$ V_2 = V_r + V_s + V_b \qquad [45] $$

Because all of the quantities are known except the radius of deformation, the equation is solved using Newton's method to find a solution for r corresponding to the volume. This is repeated until the total radius of deformation is 90% of the bottom radius. The volume of the material laid on the bottom and the side wall is calculated using the average of thickness between the third stage initial thickness and the current thickness.

4. Special Cases of Generalized Cup

4.1 *Cylindrical Cup*

4.1.1 *Stage I*

In the case of a cylindrical cup, the angle $\alpha = 0$, and this gives the first stage of formation as a complete hemispherical dome when it contacts the side wall. The thickness distribution is evaluated using the equations in terms of time increments in steps of δt:

$$s_p = s_0 \cdot e^{-(\varepsilon_{3p})} \qquad \varepsilon_{3p} = \dot{\varepsilon}_{3p} \cdot (t + \delta t) \qquad [46]$$

The analysis is performed in time steps of δt starting from a flat circular superplastic sheet. Once thickness at the pole is known, using equation

$$\frac{s_p}{s_e} = \left(\frac{2}{\sqrt{3}}\right)^{(1+m)} \left(\frac{1}{\dot{\varepsilon}_{3p}\delta t}\right)^m \left[\ln\left(\frac{t + \delta t_{s_e}}{t_{s_e}}\right)\right]^m \qquad [47]$$

thickness at the edge can be evaluated. Thickness at the edge and the pole at any instant of time can be related to the geometry of deformation using Eq 25. The angle φ included by the spherical segment at the center can be obtained by solving:

$$s_0 = 2\left(\frac{1}{\sin\varphi}\right)^2 \left[s_p(1 - \cos\varphi) - \left(\frac{s_p - s_e}{\varphi}\right)[-\varphi\cos\varphi + \sin\varphi]\right] \qquad [48]$$

4.1.2 *Stage II*

After obtaining the pole thickness s_p at time $t + \delta t$ using Eq 26, the new edge thickness s_e at time $t + \delta t$ is obtained using Eq 17. Once the thickness at the edge and the pole are determined, other unknown geometric quantities including the sheet thickness at the point of contact is obtained by solving the following set of equations:

$$^{t+\delta t}a = {}^{t}a = a \qquad [49]$$

$$^{t+\delta t}\rho = {}^{t+\delta t}a = {}^{t}a = a \qquad [50]$$

$$^{t+\delta t}q = {}^{t+\delta t}a = {}^{t}a = a \qquad [51]$$

$$s_e' = s_e - \frac{(s_e - s_p)\cdot\delta p}{\delta p + q} \qquad [52]$$

$$^{t+\delta t}V_{\text{cone}} = \pi a\,\delta p \cdot s_e + s_e' \qquad [53]$$

$$^{t+\delta t}V_{\text{dome}} = {}^{t}V_{\text{dome}} - {}^{t+\delta t}V_{\text{cone}} \qquad [54]$$

$$^{t+\delta t}V_{\text{dome}} = 2\pi a^2\left[s_p - \left(\frac{s_p - s_e}{\gamma}\right)\right] \qquad [55]$$

where $\gamma = \frac{\pi}{2}$.

4.1.3 *Stage III*

The equations for V_r, V_s, V_b, and V_2 reduce to the following when $\alpha = 0$:

$$V_r = 2\pi r r_s\left[s_e\frac{\pi}{2} - (s_e - s_p)\frac{\frac{\pi}{2}}{2}\right] + 2\pi r_s^2\left[s_p + \frac{s_e - s_p}{\frac{\pi}{2}}\right] \qquad [56]$$

$$V_2 = 2\pi\rho_2^2\left[s_p - \left(\frac{s_p - s_e}{\frac{\pi}{2}}\right)\right] \qquad [57]$$

$$V_b = \pi r^2\frac{(t + \delta t_{s_p} + t_{s_p})}{2} \qquad [58]$$

$$V_s = 2\pi a r\frac{(t + \delta t_{s_e} + t_{s_e})}{2} \qquad [59]$$

The above set of equations is solved using volume equivalents, and the radius of deformation r is obtained until the deformation reaches 90% of the bottom radius.

4.2 *Truncated Cone*

4.2.1 *Stage I*

The thickness distribution is evaluated using the equations given in an earlier section for the generalized cup. After obtaining the pole thickness s_p at time $t + \delta t$ using Eq 26, the new edge thickness s_e at time $t + \delta t$ is obtained using Eq 17. Once the thickness at the edge and the pole are determined, other unknown geometric quantities can be evaluated from the volume equivalent Eq 25. The height of deformation is checked to find if the sheet has contacted the side walls. The maximum height of deformation during stage I is given by:

$$h_1 = a\frac{(1 - \sin\alpha)}{\cos\alpha} \qquad [60]$$

4.2.2 *Stage II*

The thickness at the pole and the edge are obtained using Eq 26 and 17 and the remaining geometric and kinematic quantities are obtained using Eq 34 to 40. The thickness distribution is calculated until the height h reaches the bottom die wall.

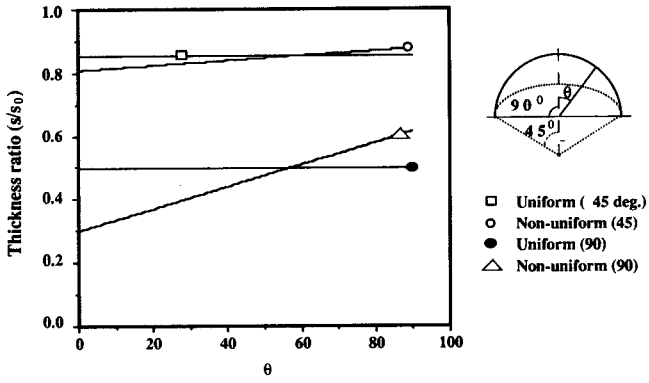

Fig. 8 Thickness comparison of uniform and nonuniform thinning models at various pole heights.

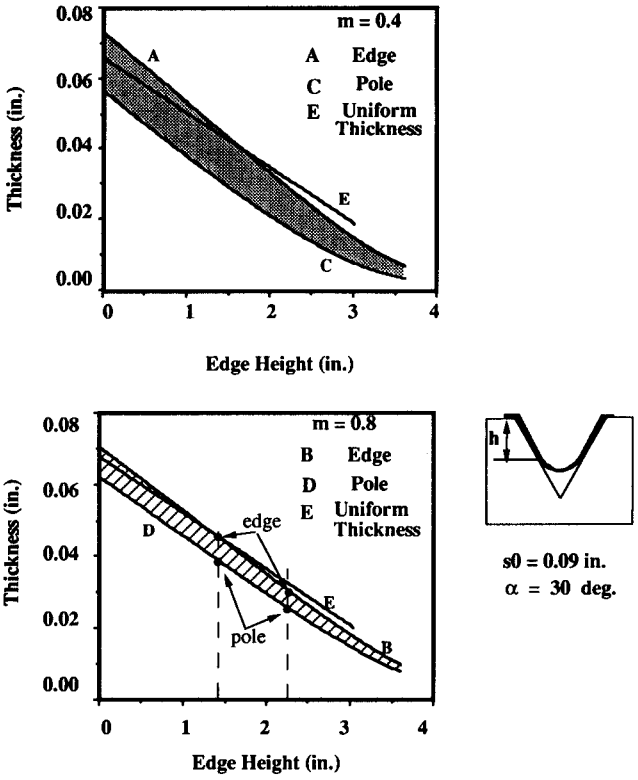

Fig. 9 Comparison of thickness profile for a cone based on uniform and nonuniform models for varying m values.

4.2.3 *Stage III*

The radius of deformation and the thickness at the edge and the pole are obtained using the Eq 17, 26, and 41 to 45, as given for stage III of a generalized cup.

4.3 *Cone*

The thickness distribution and the pressure-time cycle for a cone is given by the same set of equations as that of a truncated cone with a draft angle α. The total height of the cone H is given by the die radius a and the angle α by $a = H \tan \alpha$.

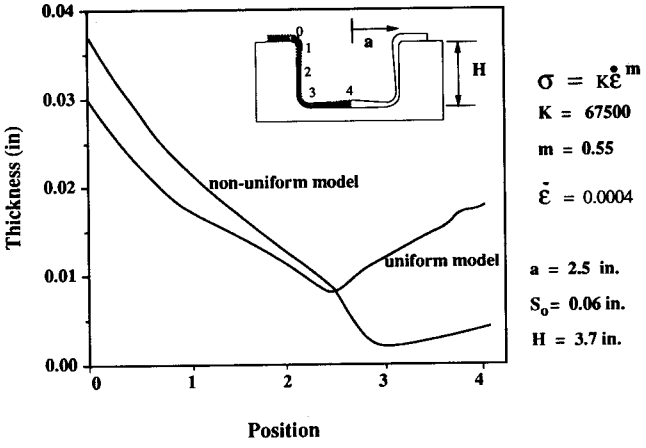

Fig. 10 Thickness profile for uniform and nonuniform models.

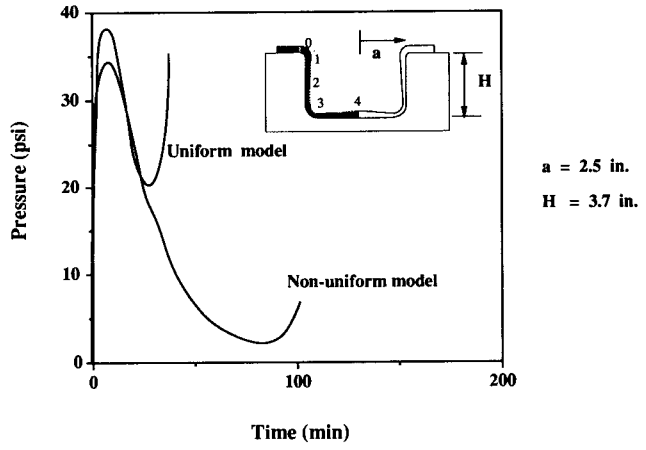

Fig. 11 Pressure-time cycle for uniform and nonuniform models.

5. Results and Discussion

The proposed nonuniform thinning distribution is used in the design and analysis of the superplastic formation of cone, right circular cylinder, and deep slanted cup. The first two examples analyze the effect of uniform and nonuniform thinning assumptions and the material properties on the forming characteristics.

Figure 8 shows the thickness profile of a free-forming dome when the dome is hemispherical (α = 90 °) and at an intermediate stage (α = 45 °). The thickness ratio s/s_0 is plotted along the convected coordinates from the pole to the edge, which can also be represented by the angle θ. s is the thickness of the dome at angle θ, and s_0 is the original thickness. When the overall deformation is less (α = 45 °), the thickness distribution predicted by both the models is close. Higher thinning (lower thickness) at the pole and lower thinning (higher thickness) at the edge are predicted by the nonuniform model. The deviation increases significantly with deformation, as can be seen in the lower part of Fig. 8 when the dome reaches hemispherical (α = 90 °).

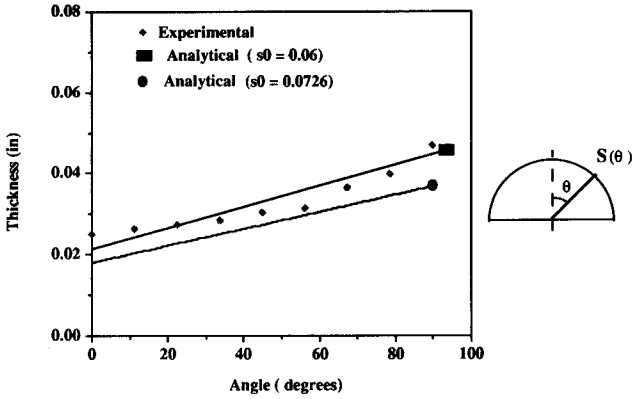

Fig. 12 Thickness variation in superplastic aluminum 7475 dome.

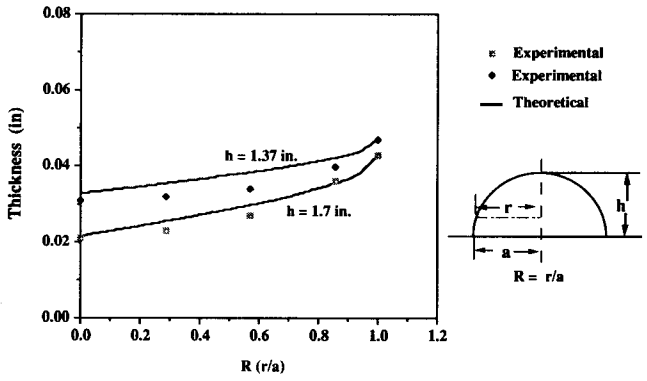

Fig. 13 Thickness profile at various pole heights, experiments and model.

The effect of strain-rate sensitivity index m on the thinning of an axisymmetric cone is shown in Fig. 9. The cone has a half cone angle of 30 ° with a radius of 2.5 in. The material is modeled with $\sigma = K\dot{\varepsilon}^m$ with $K = 28800$ lbf/(in.^{2} sec ^{m}), $m = 0.48$, $\dot{\bar{\varepsilon}} = 0.0007$/s and an initial thickness of 0.09 in. As clearly shown in Part I, the uniform thinning model is kinematic in nature, and the final thickness distribution is insensitive to m. However, in the nonuniform thinning model, the thickness at any given instant at the edge and the pole are different and are both sensitive to m.[14] The shaded regions in Fig. 9 indicate the thinning for the nonuniform thinning model and show the thickness at the edge, pole, and in-between the free-forming region. Thus, the shaded region indicates the thickness range, with the top line corresponding to the final (edge) thickness profile. The shaded region in the case of $m = 0.4$ is larger than that of $m = 0.8$, which proves that the thickness variation increases with a decrease in m (less superplastic). As can be expected, there is always a cross over of thickness profile to satisfy the equivalency of volume in the two models.

A nonmonotonic thickness distribution is observed whenever there is side and bottom contacts, as in the case of the cylindrical cup shown in Fig. 10. It can be seen that the thickness variation in a nonuniform model is greater than that of a uniform model and that the cross over of the two curves establishes

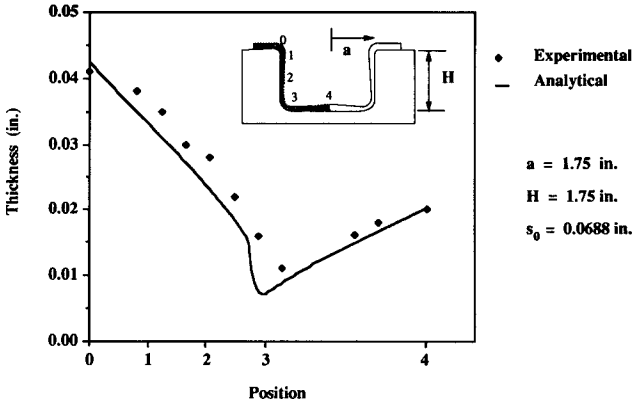

Fig. 14 Comparison of thickness profile of a completely formed cylindrical cup for aluminum 7475.

the volume constancy criteria. The pressure-time required to maintain the constant $\dot{\bar{\varepsilon}}_{opt}$ of 0.0004/s in both the models is shown in Fig. 11. Because $p \propto \frac{\sigma s}{\rho}$, the lower thickness at the pole in the nonuniform model results in a lower pressure. Also, the total time required to form increases because the material forms only around the pole region under optimal conditions. Consequently, in the nonuniform model, there is a decrease in pressure and an increase in time. The same trend is observed in all cases of generalized cup.

As a part of a research effort, domes were formed on superplastic aluminum 7475 alloy (supplied by Kobe Steel, Japan) at General Dynamics, Fort Worth Division. Hemispherical domes were formed with a radius of 3 in. held within a 4 in. rectangular die region. The material was modeled using a power-law equation, with $K = 67500$ lbf/(in.^{2} sec^m), $m = 0.55$, and an initial thickness of $s_0 = 0.06$. The thickness of the dome after it was formed is compared with the analytical results, as shown in Fig. 12. Because the entire analytical thickness distribution remains below the experimental values, the actual volume of the material in the dome is obviously more than the theoretical one. This discrepancy can be explained if additional material has flowed from the flange region into the dome, which was confirmed by actual measurement of the thickness across the flange region. If the measured $s_0 = 0.0726$ (estimated based on the dimensions of the flange and dome) were to be used, then the agreement between the numerical and experimental results improve greatly, as shown in the top line of Fig 12.

The next experimental comparison involves the formation of a cylindrical cup with aluminum 7475 alloy (supplied by Alcoa). The thickness profiles of the cup are compared with the numerical results during various stages of formation (stage I and III). During the formation of the dome (stage I), the experimental thickness at the pole height of 1.37 and 1.7 in. are shown in Fig. 13. The actual thickness along the convected coordinates is plotted against the ratio of horizontal distance r and radius a. In Fig. 14, the thickness profile for a completely formed cylindrical cup is compared with the analytical results generated by the nonuniform thinning model. The plot between the

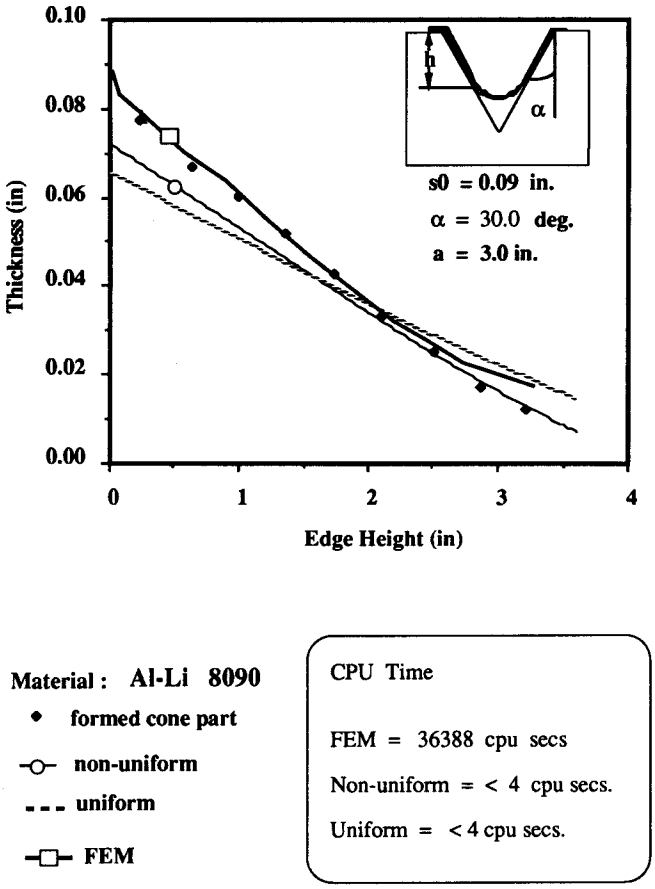

Fig. 15 Experimental and analytical results for a cone (LTV Aerospace Corporation, Fortworth Division).

thickness along the side and the bottom wall of a cylindrical cup is shown. There is slightly higher thinning in the case of the analytical results compared to that of the experimental results.

The final example involves the formation of superplastic aluminum-lithium 8090 alloy (supplied by Alcan) into a cone. The final formed thickness profile of the cone is compared with uniform and nonuniform thinning models. Agreement between nonuniform thinning and the experiment is closer, particularly in the thinnest regions of the cone. The figure also shows the results of finite-element analysis. The code SPASM[15,16]used 12 eight-noded isoparametric continuum elements to model the forming processes.

Figure 15 also shows the computational effort involved in the various models. The uniform thinning model and finite-element methods were run on VAX station 2000 using Fortran, whereas the nonuniform thinning model was run on a Macintosh IIcx using symbolic language *Mathematica*. Some benchmark problems were run on both the Mac IIcx and VAX workstation to compare the equivalent *cpu* times on the VAX workstation 2000. Comparisons were based on equivalent of time on the VAX workstation by using a conversion factor. It is very clear from the figure that uniform thinning (part I) and nonuniform thinning models (part II) are excellent design tools for superplastic forming, whereas a finite-element model is aptly suited for analysis.

8. Acknowledgement

The authors wish to acknowledge the National Science Foundation and General Dynamics Corporation for their financial support during the course of this research.

References

1. N. Chandra and D. Kannan, Superplastic Sheet Metal Forming of a Generalized Cup, PartI: Uniform Thinning, *J. Mater. Eng. Perform.*, Vol 2(No. 1), Feb 1993.
2. F. Jovane, An Approximate Analysis of the Suyperplastic Forming of a Thin Circular Diaphragm: Theory and Experiments, *Int. J. Mechan. Sci.*, Vol 10, 1968, p 403.
3. D.L. Holt, Analysis of the Bulging of a Superplastic Sheet by Lateral Pressure, *Int. J. Mechan. Sci.*, Vol 12, 1970, p 491.
4. G.C. Cornfield and R.H. Johnson, The Forming of Superplastic Sheet Metal, *Int. J. Mechan. Sci.*, Vol 12, 1970, p 479.
5. S.T.S. Al-Hassani, G.G.W. Clemas, and T.Y.M. Al-Naib, The Free Bulge Forming of Zn-Al Superplastic Sheet from a Circular Die, *Proc. 18th Int. Machine Tool Design and Research Conf.*, J.M. Alexander, Ed., London, 1977, p 361.
6. Z.X. Guo, J. Pilling, and N. Ridley, Bulge-Forming of Domes: A Comparison of Theoretical Prediction and Experiment, in *Superplasticity and Superplastic Forming*, C.H. Hamilton and N.E. Paton, Ed., The Minerals, Metals and Materials Society, 1988, p 303.
7. A.K. Ghosh and C.H. Hamilton, Superplastic Forming of a Long Rectangular Box Section Analysis and Experiment, *Proc. ASM Process Modeling Fundamentals and Applications to Metals*, ASM, 1978, p 303.
8. D. Viswanathan, S. Venkataswamy, and K.A. Padmanabhan, Theoretical and Experimental Studies on the Pressure Thermoforming of Hemispheres of Alloy Ti-6Al-4V, in *Superplasticity and Superplastic Forming*, The Minerals, Metals and Materials Society, 1988, p 321.
9. D.-J. Zhou and J. Lian, Numerical Analysis of Superplastic Bulging for Cavity-Sensitive Materials, *Int. J. Mechan. Sci.*, Vol 29, 1987, p 565.
10. Y.Q. Song and J. Zhao, A Mechanical Analysis of the Superplastic Free Bulging of Metal Sheet, *Mater. Sci. Eng.*, Vol 84, 1986, p 111.
11. A.R. Ragab, Thermoforming of Superplastic Sheet in Shaped Dies, *Met. Technol.*, Vol 10, 1983, p 340.
12. N. Chandra, Physical Modeling of Superplastic Forming, in *Light-Weight Alloys for Aerospace Applications*, E.W. Lee, E.H. Chia, and N.J. Kim, Ed., The Minerals, Metals and Materials Society, 1989, p 433.
13. A.K. Ghosh and C.H. Hamilton, On Constant Membrane Stress Test for Superplastic Metals, *Metall. Trans.*, Vol 11A, 1980, p 1915.
14. N. Chandra, D. Kannan, R.E. Goforth and L. Phillips, Mechanical Characterization of Superplastic Materials Using Modified Cone Test. Superplasticity in Aerospace II, H.C. Heikkenen and T.R. McNelley, Ed., p 67-86, TMS Publishers, 1990.
15. N. Chandra and S.C. Rama, Application of Finite Element Method to the Design of Superplastic Forming Processes, *ASME J. Eng. Ind.*, 1990.
16. N. Chandra, Finite Element Analysis of Superplastic Metal Forming Processes, Ph.D. dissertation, Texas A & M University, 1986.